Rare Metal Materials and Engineering
Volume 50, Issue 7, July 2021
Available online at www.rmme.ac.cn

Science Press

Cite this article as: Wu Xiaoyan, Zhang Huarui, Zhang Hu, et al. Quantitative Relationship Analysis Between Mechanical Properties and Microstructures of Al-7Si Aluminum Alloys by Artificial Neural Network[J]. Rare Metal Materials and Engineering, 2021, 50(07): 2329-2336.

ARTICLE

Quantitative Relationship Analysis Between Mechanical Properties and Microstructures of Al-7Si Aluminum Alloys by Artificial Neural Network

Wu Xiaoyan[1], Zhang Huarui[2], Zhang Hu[2], Wu Yanxin[1], Mi Zhenli[1], Jiang Haitao[1]

[1] National Engineering Research Center of Advanced Rolling Technology, University of Science and Technology Beijing, Beijing 100083, China; [2] School of Materials Science and Engineering, Beihang University, Beijing 100191, China

Abstract: An artificial neural network model with high accuracy and good generation ability was developed to predict and optimize the mechanical properties of Al-7Si alloys. The results show that Al-7Si alloys with tensile strength of 310~350 MPa, elongation of 3%~12%, and different microstructures are obtained by controlling the holding pressure (85~300 kPa) and cooling rate (1~10 k/s) of the casting process. The quantitative correlation relationships of the mechanical properties with microstructures of the secondary dendrite arm spacing (18.56~33.04 μm), area of eutectic Si phase (6.37~13.37 μm^2), area fraction of porosity defects (0%~0.363%), and area fraction of maximum Fe-rich intermetallics (0%~0.06%) in the alloy were established. The individual and combined influences of these microstructure characteristics on the mechanical properties were simulated. Both tensile strength and elongation are inversely related to the above-mentioned structural characteristics, and the presence of defects and Fe-rich intermetallics have great adverse effects on the properties of the alloy. Therefore, narrowing the dendrite spacing (<20 μm), modifying the eutectic Si phase (<12 μm^2), and controlling the porosity defects (<0.35%) and the morphology of the Fe-rich intermetallics are keys to prepare high-performance aluminum alloys.

Key words: aluminum alloy; artificial neural network; quantitative relationship; mechanical properties; microstructure characteristic

Al-7Si aluminum alloy has been widely used in the automotive field due to its excellent formability, high corrosion resistance and good comprehensive mechanical properties[1]. It is widely accepted that the mechanical properties of Al-7Si cast alloy are controlled by the physical metallurgy, such as the chemical composition, morphology and size of α-Al primary phase, silicon particles, and defects (porosities and Fe-rich intermetallics) [2-4]. During the actual production process, due to the problems of raw materials and casting processes, the alloy has porosity defects and many harmful iron phases, which is urgent to be resolved[5,6]. In order to achieve the goal of lightweight in the automotive field, it is of great significance to reduce automobile mass with the improvement of alloy performance. Many efforts have been made to explore the relationship between mechanical properties and microstructures of aluminum alloys[7-11]. However, all these experimental investigations reported the relationship of mechanical properties with microstructures independently and qualitatively. In addition, it is very difficult to design experiments to study their synthetic functions on mechanical properties.

Artificial neural network (ANN) is a data-driven computing method using computer technology to simulate the working mode of the human brain[12]. It has achieved significant results in the fields of speech recognition, autonomous driving, and artificial intelligence[13,14]. In recent years, the artificial neural networks to establish nonlinear relationship models in the field of materials science has been successfully applied. Haghdadi et al[15] applied ANNs for prediction of the high temperature rheological behavior of A356 aluminum alloy. The compression deformation behavior of Al-Cu-Mg-Ag alloy was also predicted and the ANN model was more accurate

Received date: July 02, 2020
Foundation item: Fundamental Research Funds for the Central Universities (FRF-TP-19-083A1); Aviation Science Foundation Project (20181174001); Guangxi Special Funding Program for Innovation-Driven Development (GKAA17202008)
Corresponding author: Jiang Haitao, Ph. D., Professor, National Engineering Research Center of Advanced Rolling Technology, University of Science and Technology Beijing, Beijing 100083, P. R. China, Tel: 0086-10-62332598, E-mail: jianght@ustb.edu.cn

than the constitutive model[16]. Canakci et al[17] established an ANN model with average absolute percentage error of about 2% to predict the effect of size and fraction of strengthened particles on the mechanical properties of the composite. Lin et al[18] combined experiments and back-propagation (BP) ANN to study the effect of heat treatment system on the tensile properties of 2A97 Al-Li alloy. Liu[19] and Wu[20] et al established the predictive model about the relationship between mechanical properties with heat treatment techniques for Al-Zn and Al-Si alloys, respectively. Emadi et al[21] compared ANN and linear regression models and obtained a model with less standard error and higher prediction accuracy. All these researches suggest that ANN models can study the relationship between complex influences and interactions qualitatively in the material research field. Therefore, this research used ANN technique to investigate the quantitative expression and the complicated nonlinear relationship between mechanical properties and microstructure of the Al-7Si cast alloy.

In this study, Al-7Si alloys with different mechanical properties and microstructures were prepared through modifying material processing techniques. The main purpose of this study is to use ANN to establish the relationship model between room temperature mechanical properties and microstructure characteristics, providing a new method for designing the alloy with targeted mechanical properties. Thus, an accurate ANN model was constructed and the quantitative relationships between the microstructures and mechanical properties of Al-7Si alloys were established.

1 Experiment

The Al-7Si aluminum alloy was used as the base material and its composition is presented in Table 1. In order to obtain the alloys with different mechanical properties and microstructures, the holding pressure (85~300 kPa) and cooling rate (1~10 k/s) were controlled during the low pressure die casting process. The tensile specimens were machined with the gage length of 30 mm and cross section diameter of 6 mm, as presented in Fig. 1. Tensile tests were conducted according to the ASTM B557 standard using an Instron 8801 universal electromechanical testing system and the ramp rate of extension was 1 mm/min. The number of tensile specimens was 51 and corresponding mechanical properties were obtained. Optimal microscopy (OM), scanning electron microscopy (SEM), and electron probe microscopy analysis (EPMA) were employed to characterize the microstructure of Al-7Si alloys. Finally, the Image-Pro Plus software (IPP 6.0) was used to investigate the characteristics of secondary dendrite arm spacing (SDAS), eutectic Si particles, Fe-rich intermetallics, and porosity defects.

Table 1 Composition of Al-7Si alloys (wt%)

Si	Mg	Ti	Sr	Fe	Al
6.910	0.297	0.117	0.017	0.144	Bal.

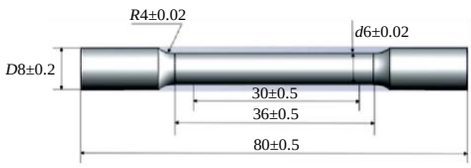

Fig.1 Schematic diagram of tensile specimen (unit: mm)

2 Results and Discussion

2.1 Characterization of microstructures and mechanical properties

The inputs and outputs for the ANN model were microstructure characteristics and mechanical properties, respectively. Representative microstructure characteristics of Al-7Si aluminum alloys obtained by different test machines are shown in Fig. 2. The microstructure of Al-7Si aluminum alloy mainly consists of primary α-Al solid solution, eutectic mixture of aluminum and silicon, Fe-rich intermetallics, and porosity defects. Therefore, the characterizations of microstructures were investigated by measuring the SDAS, size of eutectic Si particles, Fe-rich intermetallics, and porosity defects. And the variation range of morphology characteristics are shown in Table 2. The range of mechanical properties are 310~350 MPa for ultimate tensile strength (UTS) and 2.46%~12.14% for elongation (EL). The statistical results of mechanical properties, such as UTS, EL, and yield strength (YS) with SDAS are presented in Fig. 3. According to the results obtained from IPP 6.0 software, the SDAS is 18.56~33.04 μm, the area of eutectic Si phase is 6.37~13.37 μm^2, the area fraction of porosity defects is 0%~0.363% and the area fraction of maximum Fe-rich intermetallics is 0%~0.06%.

The index of relative importance (I_{RI}) of microstructures on mechanical properties of Al-7Si alloys can be calculated based on Eq.(1) and the results are presented in Fig.4. The larger the absolute value of I_{RI}, the stronger the degree of relationship between the input and output variables[22,23].

$$I_{RI} = \left| \frac{1}{N} \sum_{j=1}^{N} \frac{\Delta O}{\Delta I} \right| \quad (1)$$

where N is the number of output data; ΔO and ΔI are the percentage changes in output and input data, respectively.

The statistic results indicate that for the UTS and EL, the order of I_{RI} of sensitive factors is SDAS>area fraction of maximum Fe-rich intermetallics>Si area>area fraction of porosity defects.

2.2 ANN modeling

A multilayer ANN with a BP learning algorithm was employed to simulate the relationship between the mechanical properties and microstructure characteristics in this research using the neural network toolbox available with Matlab software. Different microstructure characteristics (SDAS, area fraction of maximum Fe-rich intermetallics, Si area, and area fraction of porosity defects) were considered as different layers in the ANN modeling. All the layers were made up with compute units and connected by transfer functions. The details

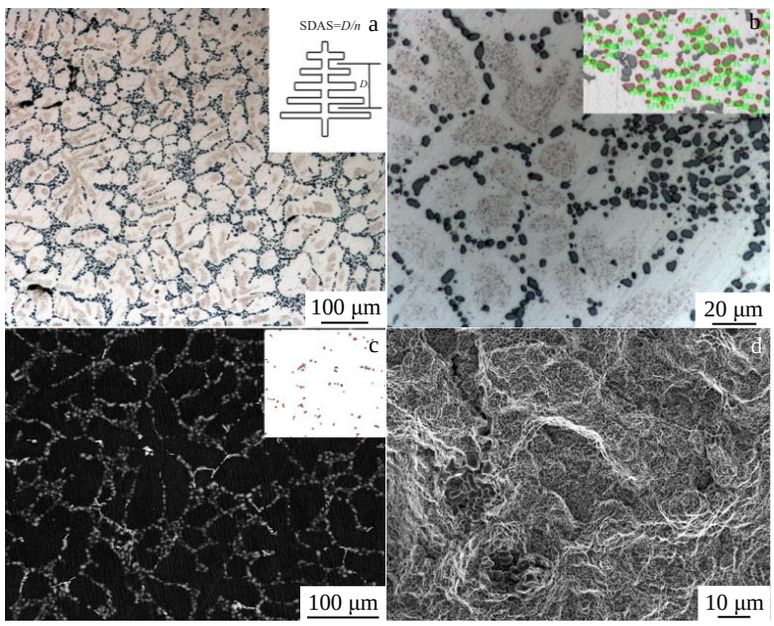

Fig.2 Microstructure characteristics of Al-7Si alloys: (a) SDAS; (b) eutectic Si phase; (c) Fe-rich intermetallics; (d) porosity defects (insets are corresponding statistical results)

Table 2 Related parameters of microstructure and properties

	Parameter	Minimum	Maximum
Input	SDAS/μm	18.56	33.04
	Area fraction of maximum Fe-rich intermetallics/%	0.003	0.055
	Si area/μm^2	6.37	13.37
	Area fraction of porosity defects/%	0	0.363
Output	UTS/MPa	310.8	350.8
	EL/%	2.46	12.14

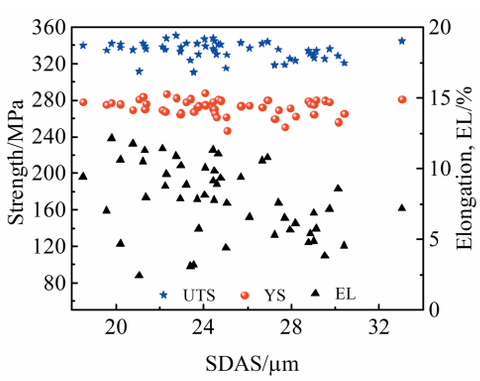

Fig.3 Relationship between mechanical properties and SDAS

of the neural network methodology and comprehensive treatments based on ANN have been reported previously[20]. In the current study, many neural networks with different numbers of neurons in the hidden layer and different transfer functions were trained to optimize the architecture. The optimum transfer function connecting these four layers can be expressed by Eq.(2)[24]:

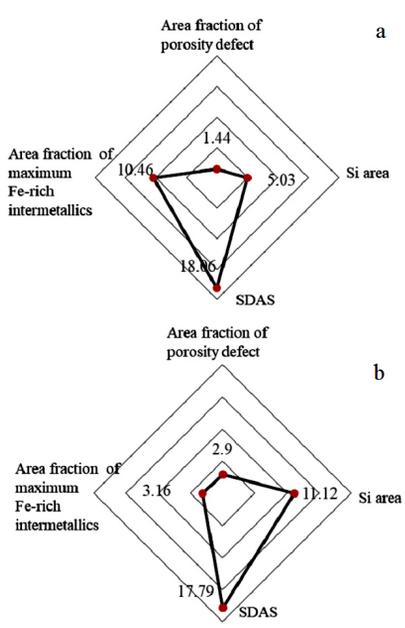

Fig.4 Influence of input parameters on UTS (a) and EL (b)

$$\text{tansig}(n)=\frac{2}{1+e^{-2n}}-1 \quad (2)$$

where n is a parameter determined by the mass matrix and threshold obtained by the ANN model. After training, it is found that the optimum model with 4-11-11-2 type architecture is adequate. Table 3 presents the parameters used in this ANN model. The ANN with the best correlations for UTS and EL was established and the ANN model designed for this study is presented in Fig.5.

2.3 Prediction of mechanical properties

2.3.1 Prediction of mechanical properties with single factor

The superior mechanical properties are related to the finer microstructural features. The effect of a single factor among microstructure characteristics on the mechanical properties is predicted in a reasonable range.

Table 3 Related parameters of ANN model

Parameter	Value
Number of layers	Input layer: 1, hidden layer: 2, output layer: 1
Number of neurons	Input neurons: 4; hidden neurons: 11, 11; output neurons: 2
Initial mass and bias	Randomly between -1~1
Learning algorithm	Traingdm
Learning rate	0.01
Activation function	tansig
Number of interactions	654
Acceptable mean-squared error	0.001
Number of specimens	51

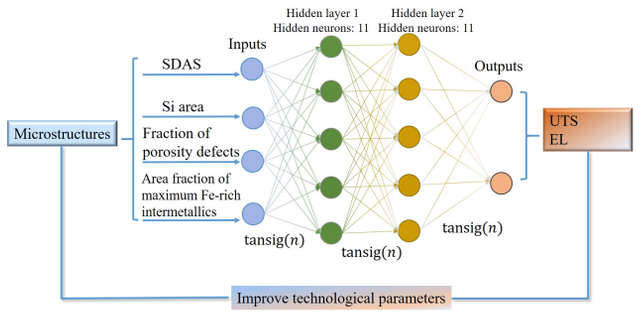

Fig.5 Schematic diagram of designed ANN model

Fig. 6 and 7 show the variation of mechanical properties with SDAS, Si area, area fraction of porosity defects, and area fraction of maximum Fe-rich intermetallics. It can be seen from Fig. 6 and 7 that the all four parameters have greater influences on the mechanical properties. The UTS and EL tend to decrease with increasing the size and fraction of these microstructural parameters. Thus UTS and EL are negatively correlated with these various factors, which is consistent with the previous sensitivity analysis results. In addition, the evolution trend of EL with microstructure characteristics is more obvious, indicating that EL is more sensitive to these four microstructure characteristics.

2.3.2 Prediction of mechanical properties with multi-factors

The influence of microstructure characteristics on mechanical properties is complex and interdependent. It is of

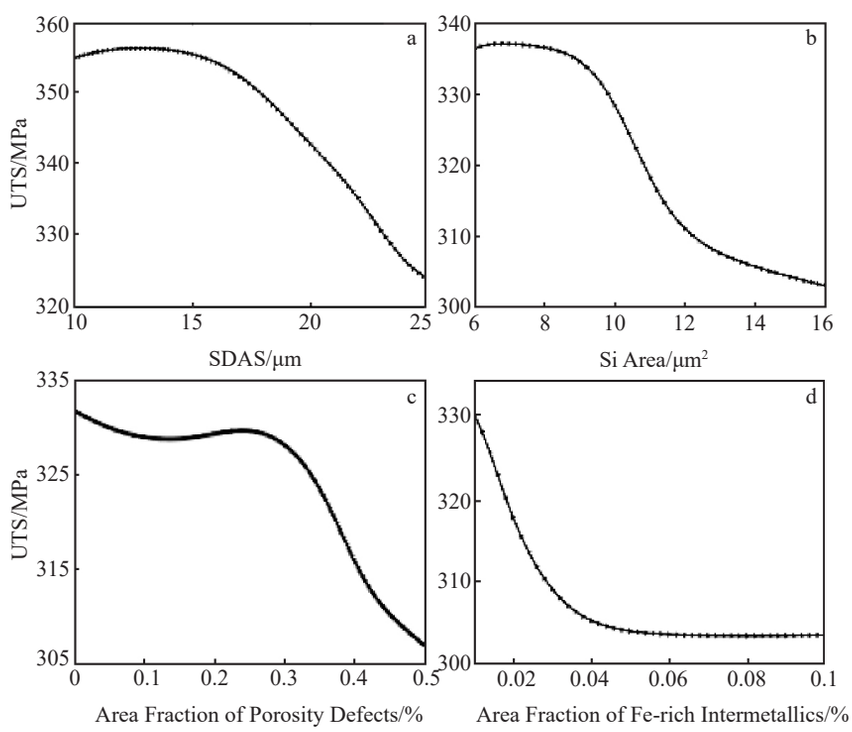

Fig.6 Predicted UTS with single factor of microstructure characteristics: (a) SDAS; (b) Si area; (c) area fraction of porosity defects; (d) area fraction of maximum Fe-rich intermetallics

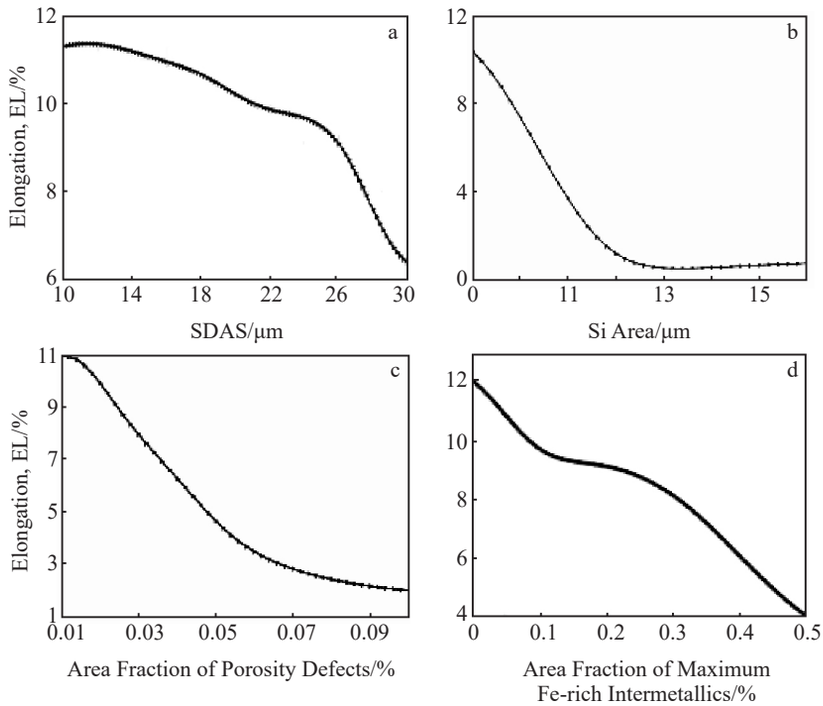

Fig.7 Predicted EL with single factor of microstructure characteristics: (a) SDAS; (b) Si area; (c) area fraction of porosity defects; (d) area fraction of maximum Fe-rich intermetallics

great importance to examine the synthetic influence of these microstructural parameters. Accordingly, the mechanical properties were simulated as a function of synthetic effects of microstructures and the 3D prediction results of the influence of microstructures on UTS and EL are presented in Fig.8 and 9, respectively.

It can be seen that a proper value of SDAS and Si area should be used to obtain the desired comprehensive mechanical properties. The effect of SDAS and eutectic Si phase area on UTS and EL is less obvious than that of area fraction of maximum Fe-rich intermetallics and porosity defects. The results indicate that controlling the impurity and defects during the alloy melting and solidification process can improve the alloy microstructure. In order to obtain Al-7Si alloys with optimal mechanical properties, a reasonable range of microstructure characteristics of the alloy was determined by ANN model. The SDAS and the Si phase area should be less than 20 μm and 12 μm^2, respectively, which is related to the casting process and the content of refiner and modifier. Besides, it is necessary to strictly control the content and morphology of Fe impurities and porosity defects in aluminum alloys. In summary, the comprehensive mechanical properties can be obtained for the Al-7Si alloy with the SDAS <20 μm, the area of eutectic Si particles <12 μm^2, the area fraction of porosity defects <0.35%, and restricted morphology of Fe-rich intermetallics, when UTS and EL are more than 350 MPa and 10%, respectively.

2.4 Quantitative relationship between mechanical properties and variables

The ANN model is a combination of a mathematical function and associated mass among inputs, hidden units, and outputs[25]. The quantitative relationships between mechanical properties (UTS and EL) and microstructure characteristics (SDAS, Si area, area fraction of maximum Fe-rich intermetallics, and porosity defects) were established, and

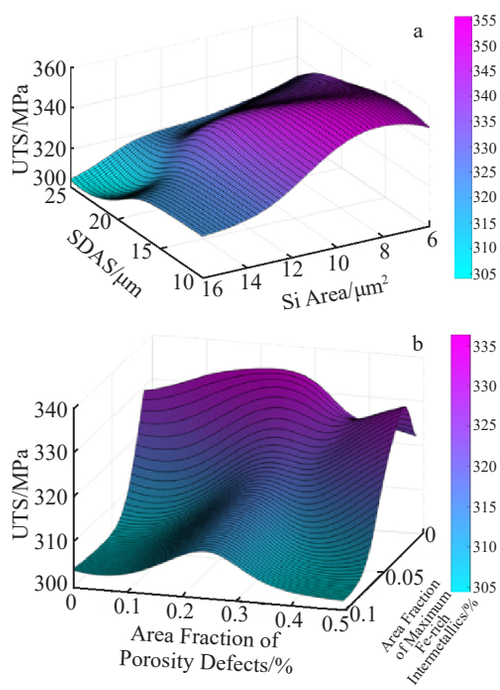

Fig.8 Predicted UTS with multi-factors of microstructure characteristics: (a) SDAS and Si area; (b) area fraction of porosity defects and maximum Fe-rich intermetallics

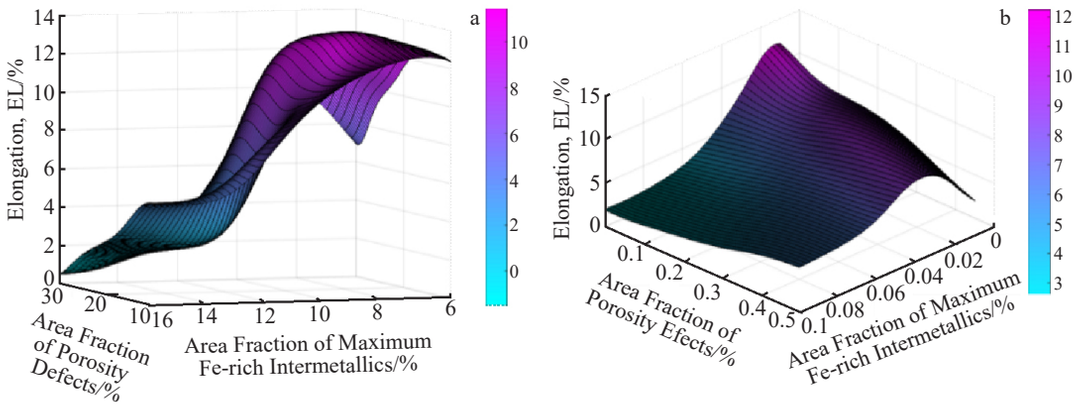

Fig.9 Predicted EL with multi-factors of microstructure characteristics: (a) SDAS and Si area; (b) area fraction of porosity defects and maximum Fe-rich intermetallics

equations of the mechanical properties with the second hidden layer are shown in Eq.(3~8).

2.4.1 Relationship between UTS and variables

The relationship between UTS and variables can be expressed by Eq.(3) as follows:

$$\mathrm{UTS} = \frac{2}{1 + e^{-2(\sum \lambda_i H_i + 0.14)}} - 1 \quad (3)$$

where i (i=1, 2, 3⋯11) represents different neuron; λ_i is the mass of each neuron shown in Table 4; H_i is the output of each neuron in the second hidden layer, which can be calculated by the quantitative relationship between the first hidden layer and the second hidden layer, as expressed by Eq.(4):

$$H_i = \frac{2}{1 + e^{-2(a_i E_1 + b_i E_2 + c_i E_3 + d_i E_4 + e_i E_5 + f_i E_6 + g_i E_7 + h_i E_8 + i_i E_9 + j_i E_{10} + k_i E_{11} + l_i)}} - 1 \quad (4)$$

where E_i is the output of each neuron in the first layer, which can be calculated by Eq.(5); the letters a_i~k_i represent the mass; l_i is the threshold. The related values are shown in Table 4.

$$E_i = \frac{2}{1 + e^{-2(\alpha_i M_1 + \beta_i M_2 + \gamma_i M_3 + \delta_i M_4 + f_i)}} - 1 \quad (5)$$

where M_1~M_4 are the input parameters, f_i is the threshold, and the letters α_i~δ_i are mass shown in Table 5.

2.4.2 Relationship between EL and varibles

The relationship between EL and variables can be expressed by Eq.(6) as follows:

$$\mathrm{EL} = \frac{2}{1 + e^{-2(\sum \lambda_i H_i + 0.55)}} - 1 \quad (6)$$

The values of λ_i for EL simulation are shown in Table 6. H_i for EL simulation can be calculated by the quantitative

Table 4 Coefficient of the second hidden layer and the first hidden parameters of quantitative equations for UTS simulation

i	1	2	3	4	5	6	7	8	9	10	11
a_i	0.60	-0.57	-0.46	0.35	0.66	0.53	-0.41	-0.86	-0.14	0.85	0.18
b_i	-0.06	0.51	0.72	0.70	-0.94	0.73	0.85	0.16	0.53	-0.69	0.11
c_i	-0.69	-0.37	0.54	0.62	0.11	0.26	-0.42	0.72	-0.69	0.38	-0.82
d_i	0.53	-0.61	0.16	0.27	-0.70	-0.27	-0.46	0.34	-0.76	0.63	-0.21
e_i	-0.57	-0.41	-0.26	-0.71	-0.27	-0.22	0.15	-0.90	-0.62	-0.71	-0.17
f_i	-0.78	-0.76	-0.95	-0.40	-0.06	-0.83	-0.39	-0.17	-0.53	0.11	-0.29
g_i	-0.42	0.45	0.11	0.72	0.10	0.58	0.18	0.08	0.85	-0.15	0.05
h_i	0.83	-0.72	-0.41	0.64	0.92	-0.80	-0.01	0.28	0.34	0.55	0.93
i_i	0.01	0.42	-0.88	0.12	-0.40	0.31	-0.58	0.75	-0.18	-0.59	0.31
j_i	-0.03	-0.18	0.01	-0.36	0.21	-0.20	0.88	-0.17	0.06	-0.20	-0.42
k_i	0.52	-0.64	0.08	0.48	0.01	0.54	-0.71	-0.44	0.49	0.17	-1.01
l_i	-1.72	1.35	1.16	-0.70	-0.35	-0.09	-0.31	-0.71	-0.99	1.35	1.74
λ_i	-0.77	0.56	0.60	0.04	-0.16	0.82	0.57	-0.66	-0.72	0.71	0.18

Table 5 Coefficient of the first hidden layer and the input parameters of quantitative equations for UTS simulation

i	1	2	3	4	5	6	7	8	9	10	11
α_i	2.05	0.54	-0.53	0.73	-0.94	-0.18	-1.31	-1.5	-1.13	1.11	-0.46
β_i	0.47	-0.92	0.63	-0.04	0.09	0.19	-0.99	1.02	-1.72	-1.16	-1.08
γ_i	-0.79	1.95	1.23	1.01	0.68	-1.37	-0.77	-1.42	-0.69	-0.73	1.24
δ_i	0.17	-0.03	0.81	-1.46	1.98	-0.02	-0.31	-0.21	-0.40	1.33	-1.16
f_i	-2.26	-1.87	1.44	-0.90	0.47	0.00	-0.69	-0.77	-1.15	1.87	-2.29

Table 6 Coefficient of the second hidden layer and the first layer parameters of quantitative equations for EL simulation

i	1	2	3	4	5	6	7	8	9	10	11
a_i	0.39	0.42	0.40	-0.55	-0.54	-0.49	0.72	-0.15	1.00	-1.11	0.39
b_i	-1.11	0.24	0.42	-0.55	0.73	-0.13	0.48	0.16	0.72	0.10	-1.11
c_i	0.72	-0.19	0.87	0.67	0.20	0.63	-0.52	0.58	0.39	-0.35	0.72
d_i	-0.79	0.87	-0.40	-0.15	0.26	0.67	0.80	-0.75	0.88	0.05	-0.79
e_i	0.33	-0.03	0.84	0.18	-1.06	-0.78	0.04	-0.86	0.28	0.63	0.33
f_i	0.18	-0.60	0.49	-0.25	0.25	-0.29	0.60	0.65	0.32	-0.40	0.18
g_i	0.34	-0.54	0.77	0.47	-0.23	-0.28	0.83	0.45	-0.32	0.26	0.34
h_i	-0.37	-0.79	0.06	-0.79	0.64	-0.23	-0.11	0.41	0.55	0.22	-0.37
i_i	-0.29	-0.73	0.37	-0.81	-0.22	0.71	-0.22	0.80	0.18	0.61	-0.29
j_i	0.31	0.61	0.26	0.71	0.87	-0.91	-0.60	0.22	0.35	-0.56	0.31
k_i	-1.76	-1.31	-0.99	0.57	0.28	-0.24	0.58	-1.04	1.35	-1.75	-1.76
l_i	0.22	-0.23	-1.52	-1.27	-0.07	1.82	1.22	0.08	0.75	-0.32	-0.80
λ_i	-0.84	1.03	0.47	-0.32	0.54	0.58	0.05	0.87	-0.37	0.74	-0.47

Table 7 Coefficient of the first hidden layer and the input parameters of quantitative equations for EL simulation

i	1	2	3	4	5	6	7	8	9	10	11
α_i	0.36	1.04	1.56	0.17	0.84	-0.16	0.45	1.35	0.28	1.58	-1.2
β_i	-0.79	1.14	-0.56	1.28	0.24	0.25	-0.89	-1.08	0.69	-0.21	0.18
γ_i	1.40	1.28	-0.44	-0.19	1.91	-1.28	1.09	0.80	1.64	-0.54	-0.71
δ_i	-1.04	0.95	-1.24	1.48	0.38	-0.70	1.38	-0.97	0.04	0.75	-1.07
f_i	-2.26	-1.87	1.44	-0.90	0.47	0.00	-0.69	-0.77	-1.15	1.84	-2.29

relationship between the first hidden layer and the second hidden layer, as expressed by Eq.(7):

$$H_i=\frac{2}{1+e^{-2(a_iE_1+b_iE_2+c_iE_3+d_iE_4+e_iE_5+f_iE_6+g_iE_7+h_iE_8+i_iE_9+j_iE_{10}+k_iE_{11}+l_i)}}-1 \quad (7)$$

E_i for EL simulation can be calculated by Eq. (8). The related values are shown in Table 6.

$$E_i=\frac{2}{1+e^{-2(\alpha_iM_1+\beta_iM_2+\gamma_iM_3+\delta_iM_4+f_i)}}-1 \quad (8)$$

The values of letters α_i~δ_i for EL simulation are shown in Table 7.

3 Conclusions

1) During the low casting process, the Al-7Si alloys with different mechanical properties and microstructure characteristics are obtained by controlling the holding pressure and cooling rate.

2) The microstructure characteristics have direct influence on the mechanical properties of Al-7Si alloy. The influential sensitivity sequence of the microstructures on the mechanical properties is established. The porosity defects and area fraction of maximum Fe-rich intermetallics are two important parameters in deteriorating the mechanical properties.

3) Based on the predicted results of the artificial neural network model, the Al-7Si alloy with the secondary dendrite arm spacing <20 μm, the area of eutectic Si particles <12 μm^2, the area fraction of porosity defects <0.35%, and controlled morphology of Fe-rich intermetallics owns the comprehensive mechanical properties. The ultimate tensile strength and elongation is more than 350 MPa and 10%, respectively.

References

1 Wu X Y, Yun Y, Zhang H R *et al*. *Materials Research Express*[J], 2017, 4(12): 126 501

2 Li D F, Cui C X, Wang X *et al*. *Materials & Design*[J], 2016, 90: 820

3 Wu X Y, Zhang H R, Chen H L *et al*. *China Foundry*[J], 2017, 14(2): 138

4 Qiu C R, Miao S N, Li X R *et al*. *Materials & Design*[J], 2017, 114: 563

5 Kim K S, Park J C, Yim C D *et al*. *Procedia Engineering*[J], 2011, 10: 165

6 Wang Q G. *Metallurgical and Materials Transactions A*[J], 2003, 34(12): 2887

7 Li J H, Suetsugu S, Tsunekawa Y *et al*. *Metallurgical and Materials Transactions A*[J], 2013, 44(2): 669

8 Kuijpers N C W, Vermolen F J, Vuik C. *Materials Science and Engineering A*[J], 2005, 394(1-2): 9

9 Dorin T, Stanford N, Birbilis N *et al*. *Corrosion Science*[J], 2015, 100: 396

10 Davami P, Varahram N, Kim S K. *Materials Science and Engineering A*[J], 2013, 565: 278

11 Wu X Y, Zhang H R, Zhang F X *et al*. *Materials Characterzation* [J], 2018, 139: 116

12 Reddy N S, Panigrahi B B, Ho C M *et al*. *Computational Materials Science*[J], 2015, 107: 175

13 Wan B B, Chen W P, Liu L S *et al*. *Materials Science and Engineering A*[J] 2016, 666: 165

14 Khalaj G, Nazari A, Yoozbashizadeh H *et al*. *Neural Computing and Applications*[J], 2014, 24(2): 301

15 Haghdadi N, Zarei-Hanzaki A, Khalesian A R *et al*. *Materials & Design*[J], 2013, 49: 386

16 Lu Z L, Pan Q L, Liu X Y *et al*. *Mechanics Research Communications*[J], 2011, 38(3): 192

17 Canakci A, Varol T, Ozsahin S. *The International Journal of Advanced Manufacturing Technology*[J], 2015, 78(1-4): 305

18 Lin Y, Zheng Z Q, Zhang H F *et al*. *Transactions of Nonferrous Metals Society of China*[J], 2013, 23(6): 1728

19 Liu J J, Li H Y, Li D W *et al*. *Transactions of Nonferrous Metals Society of China*[J], 2015, 25(3): 944

20 Wu X Y, Zhang H R, Cui H Y *et al*. *Materials*[J], 2019, 12 (5): 718

21 Emadi D, Mahfoud M. *Procedia Engineering*[J], 2011, 10: 589

22 Liu G X, Jia L N, Kong B *et al*. *Materials & Design*[J], 2017, 129: 210

23 Guan K, Jia L N, Chen X J *et al*. *Materials Science and Engineering A*[J], 2014, 605: 65

24 Nowak G, Rusin A. *Applied Thermal Engineering*[J], 2016, 108: 204

25 Ozturk S, Kayabasi E, Celik E *et al*. *Journal of Materials Science: Materials in Electronics*[J], 2018, 29(1): 260

基于人工神经网络的亚共晶Al-7Si合金力学性能与显微组织定量关系分析

武晓燕[1]，张花蕊[2]，张　虎[2]，吴彦欣[1]，米振莉[1]，江海涛[1]

(1. 北京科技大学 高效轧制国家工程研究中心，北京 100083)

(2. 北京航空航天大学 材料科学与工程学院，北京 100191)

摘　要：以亚共晶Al-7Si合金为研究对象，基于Matlab神经网络工具箱开发了铝合金性能和组织关系预测程序，获得了高精度的材料性能与组织特征的关系预测模型。通过控制增压铸造过程中保压压力（85~300 kPa）和冷却速度（1~10 k/s）参数，获得具有不同力学性能和组织特征的铝合金。拉伸试样力学性能测试结果表明：抗拉强度为310~350 MPa，延伸率为3%~12%。采用IPP 6.0软件统计组织特征参数结果表明：二次枝晶间距为18.56~33.04 μm，共晶Si相面积为6.37~13.37 μm^2，缺陷面积百分数为0%~0.363%，最大Fe相面积百分数为0%~0.06%。通过人工神经网络（ANN）预测模型，探究了单因素和双因素协同作用对合金力学性能的影响规律，建立了合金性能优化的组织控制路径。预测结果表明，该合金强度和塑性均与4种组织特征呈负相关，且缺陷和Fe相的存在对合金性能有较大的不利影响。因此，缩小枝晶间距（<20 μm）、变质共晶Si相（<12 μm^2）、控制孔洞缺陷（<0.35%）、严格控制富Fe相的尺寸和形态，是制备高性能铝合金的关键。

关键词：铝合金；人工神经网络；定量关系；机械性能；组织特征

作者简介：武晓燕，女，1989年生，博士，北京科技大学高效轧制国家工程研究中心，北京 100083，电话：010-62332598，E-mail：wuxiaoyan@ustb.edu.cn